DOI: 10.1002/chem.200700104

Structural, Kinetic, and Theoretical Studies on Models of the Zinc-Containing Phosphodiesterase Active Center: Medium-Dependent Reaction Mechanisms

Katalin Selmeczi,[a] Carine Michel,[a] Anne Milet,[a] Isabelle Gautier-Luneau,[b] Christian Philouze,[a] Jean-Louis Pierre,[a] David Schnieders,[c] Annette Rompel,[c] and Catherine Belle*[a]

Dedicated to Professor Bernt Krebs

Abstract: Dinuclear zinc(II) complexes $[Zn_2(bpmp)(\mu\text{-}OH)](ClO_4)_2$ (**1**) and $[Zn_2(bpmp)(H_2O)_2](ClO_4)_3$ (**2**) (H-BPMP = 2,6-bis[bis(2-pyridylmethyl)-aminomethyl]-4-methylphenol) have been synthesized, structurally characterized, and pH-driven changes in metal coordination observed. The transesterification reaction of 2-hydroxypropyl *p*-nitrophenyl phosphate (HPNP) in the presence of the two complexes was studied both in a water/DMSO (70:30) mixture and in DMSO. Complex **2** was not reactive whereas for **1** considerable rate enhancement of the spontaneous hydrolysis reaction was observed. A detailed mechanistic investigation by kinetic studies, spectroscopic measurements (^1H, ^{31}P NMR spectroscopy), and ESI-MS analysis in conjunction with ab initio calculations was performed on **1**. Based on these results, two medium-dependent mechanisms are presented and an unusual bridging phosphate intermediate is proposed for the process in DMSO.

Keywords: ab initio calculations · bioinorganic chemistry · phosphodiesters · reaction mechanisms · zinc

Introduction

Polynuclear zinc-containing enzymes play multifaceted roles in biological systems. Their nuclease activity is of paramount importance, for example, the phosphatediesterase activity towards RNA (RNaseH from HIV reverse transcriptase,[1] P1 nuclease[2]). That is why understanding the detailed reaction mechanisms of RNA cleavage by internal phosphoester transfer (transesterification) has focused the attention of many researchers since the first description of RNA strand scission in the 1950s.[3] Thorough comprehension of this mechanism will provide a solid basis for the rational design of more efficient artificial dinuclear phosphodiesterases as potential therapeutic agents. The zinc ion with its flexible coordination sphere, fast ligand-exchange capacity, strong Lewis acidity, lack of redox activity, and nontoxic nature appears to be the metal of choice for this purpose.

In spite of significant progress in the biomimetic complex model approach,[4–6] the overall mechanism and the substrate binding to the metal ions are still a matter of debate. The reaction starts with nucleophilic attack by the 2′-oxygen atom on the adjacent phosphorus center and yields a 2′,3′-cyclic phosphate with a 5′-terminal hydroxy group (Scheme 1). Different mechanisms for the behavior of individual zinc hydrolases have been discussed in the literature.[7,8] Three modes of catalytic activation have been proposed (Scheme 1a):[9,10] 1) Lewis acid activation: β mode, substrate coordination via one or two phosphate oxygen atom(s) to the metal(s), which also contribute to charge neutralization and pentacoordinate phosphorus stabilization; 2) intramolecular general base formation: γ mode, deproto-

[a] Dr. K. Selmeczi, C. Michel, Prof. A. Milet, Dr. C. Philouze, Prof. J.-L. Pierre, Dr. C. Belle
Département de Chimie Moléculaire, Université J. Fourier
Grenoble I, UMR-5250, ICMG FR-2607
CNRS BP-53, 38041 Grenoble (France)
Fax: (+33) 476-514-836
E-mail: catherine.belle@ujf-grenoble.fr

[b] Prof. I. Gautier-Luneau
Laboratoire de Cristallographie, Université J. Fourier
Grenoble I, UPR 5031 CNRS, 25 avenue des Martyrs, BP-166
38042 Grenoble (France)

[c] Dr. D. Schnieders, Dr. A. Rompel
Institut für Biochemie, Westfälische Wilhelms-Universität Münster
Wilhem-Klemm-Strasse 2, 48149 Münster (Germany)

Supporting information for this article is available on the WWW under http://www.chemeurj.org/ or from the author.

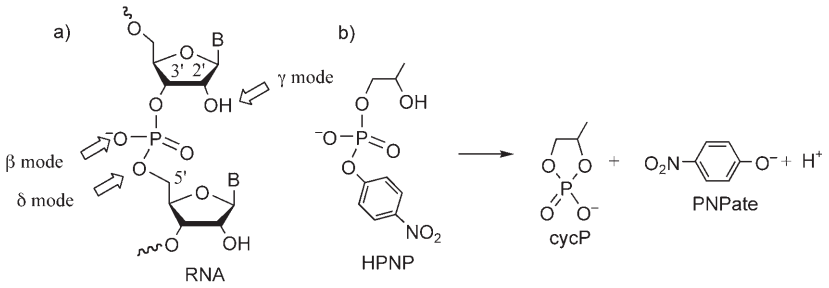

Scheme 1. a) Catalytic activation strategies to cleave RNA. b) Transesterification of 2-hydroxypropyl *p*-nitrophenyl phosphate (HPNP) as a substrate model of RNA.

nation of the 2′-hydroxy group by a metal-coordinated hydroxide; 3) intramolecular general acid formation: δ mode, interaction with the 5′-oxygen atom of the leaving group by a metal-coordinated water molecule. The main roles of the zinc ion include the generation of a hydroxide nucleophile at physiological pH by lowering the pK_a of coordinated water, the orientation and activation of the substrate through metal coordination, and the stabilization of intermediates.

To investigate further the catalytic activation mode of zinc-containing nucleases, two new dinuclear zinc complexes, $[Zn_2(bpmp)(\mu\text{-}OH)](ClO_4)_2$ (**1**) and $[Zn_2(bpmp)(H_2O)_2](ClO_4)_3$ (**2**), with the ligand 2,6-bis[bis(2-pyridylmethyl)aminomethyl]-4-methylphenol (H-BPMP) have been studied in a combined theoretical and experimental investigation. First, the complexes were synthesized, structurally characterized, and the pH-driven changes in metal coordination were analyzed in detail. Subsequently, the transesterification of 2-hydroxypropyl *p*-nitrophenyl phosphate (HPNP), an RNA model substrate, was studied in both water/DMSO (70:30) and in pure DMSO to mimic the hydrophilic/lipophilic balance in the local environment of the active site, which is an important enzyme requirement. In both media, complex **1** efficiently promotes the hydrolysis of HPNP, whereas complex **2** does not. Moreover, the kinetic data for **1** in the two media revealed different activities, which seemed to indicate the presence of different mechanisms that depend on the hydrophilic/lipophilic balance. To fulfill the need for further information on substrate/intermediate/product binding on biomimetic complexes, a multidisciplinary investigation was carried out based on spectroscopic and kinetic studies combined with full quantum theoretical calculations on the real systems. This approach has allowed us to gain more insight into the origin of the observed medium-dependent behavior. Herein, we present the structures of the intermediates, which are supported by theoretical calculations, spectroscopic data (by using ^1H, ^{31}P NMR spectroscopy), and mass spectrometric analysis (by using ESI-MS). Finally, the catalytic cycles in the two media will be discussed, providing new insights into the reactivity of these zinc complexes.

Results

X-ray crystal structures

*Dinuclear Zn^{II}–hydroxo complex **1**·THF·0.67MeCN·0.33H_2O*: Crystals that were suitable for X-ray structure determination were obtained by the slow diffusion of THF into a solution of **1** in acetonitrile at −20 °C. The unit cell also contains one molecule of the THF solvent along with MeCN and H_2O which occupy the same position in ratios of 2:3 and 1:3. The molecular structure of **1**, shown in Figure 1 with selected bond lengths and angles

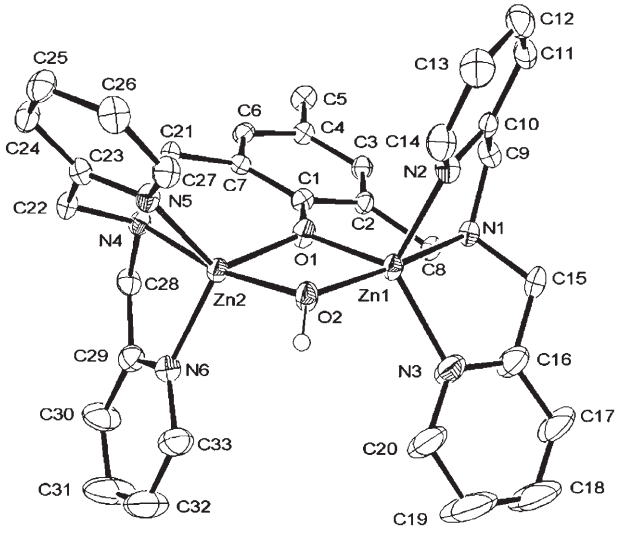

Figure 1. Ortep representation of the dicationic unit cell of **1**. Hydrogen atoms have been omitted for clarity except for the hydrogen atom of the OH bridge.

supplied in Table 1, consists of a dinuclear complex in which two Zn^{II} ions are double bridged by the phenoxo group of the BPMP ligand and by the hydroxo group. By using the method of Addison et al.[11] to determine the geometry of the pentacoordinated environment ($\tau=0$ for a regular square pyramid and $\tau=1$ for a regular trigonal bipyramid), the zinc ions can be described as adopting a distorted trigonal bipyramid geometry with $\tau=0.84$ for Zn1 and $\tau=0.93$ for Zn2. The trigonal planes in the pentacoordinated sphere of Zn1 and Zn2 are occupied by O1, N2, N3 and O1, N5, N6, in which Zn1 and Zn2 are located out of the basal plane by 0.261(0) and 0.262(5) Å, respectively, towards the O2 atom. The axial positions of Zn1 and Zn2 are occupied by O2 of the hydroxo bridge and N1 and N4, respectively, of the corresponding tertiary amine. The Zn–O lengths in the Zn_2O_2 unit are in the range of 1.986(3) to 2.032(3) Å. The four atoms, Zn1, Zn2, O1, and O2, are in the same plane with a maximal deviation from the least-square plane of

Table 1. Selected bond lengths [Å] and angles [°] for **1** from X-ray and theoretical data (*in italics*).

Zn1···Zn2	3.016(1)	*3.026(9)*	Zn2-O1	2.032(3)	*2.040(9)*
Zn1−O1	2.025(3)	*2.065(8)*	Zn2−O2	1.986(3)	*2.027(5)*
Zn1−O2	1.987(3)	*2.010(8)*	Zn2−N4	2.194(4)	*2.284(9)*
Zn1−N1	2.200(4)	*2.289(7)*	Zn2−N5	2.073(4)	*2.137(0)*
Zn1−N2	2.081(4)	*2.134(4)*	Zn2−N6	2.071(5)	*2.149(5)*
Zn1−N3	2.066(5)	*2.162(3)*			
O1-Zn1-O2	82.5(1)	*83.6(6)*	O1-Zn2-O2	82.3(1)	*83.8(8)*
O1-Zn1-N1	89.8(1)	*87.8(7)*	O1-Zn2-N4	88.3(1)	*88.6(0)*
O1-Zn1-N2	110.1(2)	*112.1(9)*	O1-Zn2-N5	125.3(2)	*127.1(5)*
O1-Zn1-N3	122.3(2)	*123.9(8)*	O1-Zn2-N6	112.4(2)	*112.1(3)*
O2-Zn1-N1	172.2(1)	*171.5(1)*	O2-Zn2-N4	168.4(1)	*167.6(2)*
O2-Zn1-N2	104.2(2)	*105.3(7)*	O2-Zn2-N5	99.6(2)	*98.2(5)*
O2-Zn1-N3	103.8(2)	*105.8(4)*	O2-Zn2-N6	110.5(2)	*113.9(3)*
N1-Zn1-N2	79.4(2)	*78.1(6)*	N4-Zn2-N5	80.2(2)	*78.4(9)*
N1-Zn1-N3	79.5(2)	*78.6(5)*	N4-Zn2-N6	79.4(2)	*78.0(1)*
N2-Zn1-N3	122.8(2)	*117.4(4)*	N5-Zn2-N6	117.5(2)	*114.6(6)*
Zn2-O2-Zn1	98.82(1)	*97.1(4)*	Zn2-O1-Zn1	96.04(2)	*94.96(2)*

0.0362 Å. The small Zn2-O1-Zn1 (96.04(2)°) and Zn2-O2-Zn1 (98.82(1)°) angles lead to a short Zn1···Zn2 distance of 3.016(1) Å compared with those of similar dibridged dinuclear zinc complexes with phenolate- (or alkoxo) and carboxylate-bridged ligands.[12,13]

Dinuclear Zn^{II}–bisaqua complex ***2*·4H_2O**: Single crystals of **2** that were suitable for X-ray structure determination were obtained from a mixture of acetone/water by slow evaporation. Four molecules of water per complex were found in the cell, and the molecular structure of the cation of **2** is shown in Figure 2. The most important interatomic bond lengths and angles are compiled in Table 2. The molecular entity possesses a two-fold symmetry axis that passes through the C5, C4, C1, and O1 atoms; the Zn and Zn′ atoms are on opposite sides of the phenolate ring plane. Each zinc ion is pentacoordinated by one tertiary amine, two pyridine groups and two oxygen atoms, one of which comes from the phenoxo bridge and the other is from a molecule of water. The coordination sphere around zinc can be described as a weakly distorted square pyramid with a τ value of 0.28. The four positions in the basal plane are occupied by the N1, N2, N3, and O2 atoms. The maximum deviation from the least-squares plane is 0.108(4) Å and the zinc atom lies 0.319(4) Å out of the basal plane. The distance from zinc to the equatorial atoms varies in a narrow range from 2.043(3) to 2.188(4) Å. The phenoxo oxygen (O1) occupies the apical position with a Zn−O1 bond length of 2.036(2) Å. The Zn-O1-Zn′ bond angle is 137.21(3)° and the intermetallic distance is 3.791(1) Å.

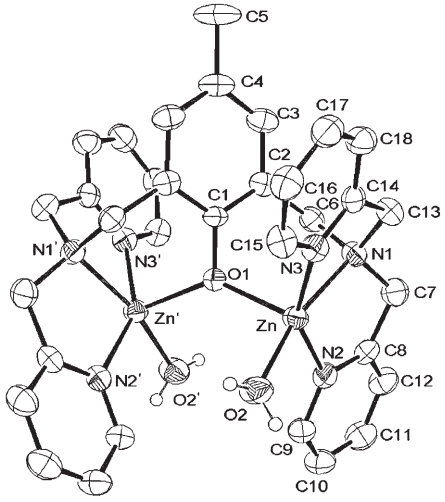

Figure 2. Ortep representation of the tricationic unit cell of **2**. Hydrogen atoms have been omitted for clarity except for the hydrogen atoms of the water molecules.

Table 2. Selected bond lengths [Å] and angles [°] for **2** from X-ray data.

Zn···Zn′	3.791(1)	Zn−N1	2.188(4)
Zn−O1	2.036(2)	Zn−N2	2.073(4)
Zn−O2	2.043(5)	Zn−N3	2.078(4)
O1-Zn-O2	99.3(1)	O2-Zn-N3	98.9(2)
O1-Zn-N1	92.9(1)	N1-Zn-N2	79.2(2)
O1-Zn-N2	104.0(1)	N1-Zn-N3	80.9(1)
O1-Zn-N3	98.1(1)	N2-Zn-N3	150.9(1)
O2-Zn-N1	167.7(1)	Zn-O1-Zn′	137.21(3)
O2-Zn-N2	96.1(2)		

^{1}H NMR spectroscopic titration: To characterize the structural changes of complexes **1** and **2** and species distribution in aqueous solution upon varying the pH, we performed a detailed ^{1}H NMR spectroscopic study in D_2O/[D_6]DMSO (70:30). The ^{1}H NMR spectrum of **1** shows eight resonances that confirms the high symmetry of the dinuclear complex. The ^{1}H NMR spectrum has a singlet for the methyl protons ($\delta = 2.0$ ppm), two multiplets for the methylene protons ($\delta =$ 3.6 and 4.0 ppm), a singlet for the two protons of the benzene ring ($\delta = 6.8$ ppm), and two doublets ($\delta = 7.4$ and 8.7 ppm) and two triplets ($\delta = 7.5$ and 7.9 ppm) that correspond to the protons of the pyridine rings (see Figure S1a in the Supporting Information). The ^{1}H NMR spectrum of **2** shows two singlets, one for the methyl protons ($\delta = 1.8$ ppm) and one for the two protons of the benzene ring ($\delta =$ 6.6 ppm). Broad resonances for the protons of the methylene group and the pyridine rings are also observed owing to fast proton exchange of the water molecules coordinated to the zinc ions on the NMR spectroscopy timescale. Upon addition of DCl to a solution of **1** (5 mM) adjusted to pH 8.5, numerous changes were observed. Decreasing the pH leads to broadening and changes in chemical shift of the signals with a concomitant decrease in intensity. At around a pH of

5, the original spectrum of **2** in D_2O/[D_6]DMSO (70:30) was obtained, and after addition of NaOD to the solution of **2** (5 mM), the spectrum of **1** was fully restored, which provides evidence for the reversible interconversion of the two species (Scheme 2). The pH-dependent (over the range of pH 6.0–8.5) ^{1}H NMR spectroscopy chemical shifts of the methyl, phenyl, and pyridinyl protons (δ) show sigmoidal behavior (Figure S2 in the Supporting Information). The pK_a was determined on the basis of a Schwarzenbach-type analysis by using the equation $\delta = \delta_b + K_a(\delta_a - \delta)/[H^+]$, in which K_a is the water deprotonation constant and δ_a, δ_b, and δ are the chemical shifts observed for species **1**, **2**, and the mixture of the two in fast exchange, respectively.[14] A pK_a value of 7.60($\pm$0.03) was obtained, which is close to the pK_a values found for other dinuclear zinc(II) complexes.[15]

Catalysis: The catalytic activity of **1** and **2** was studied for the transesterification of the RNA model substrate HPNP

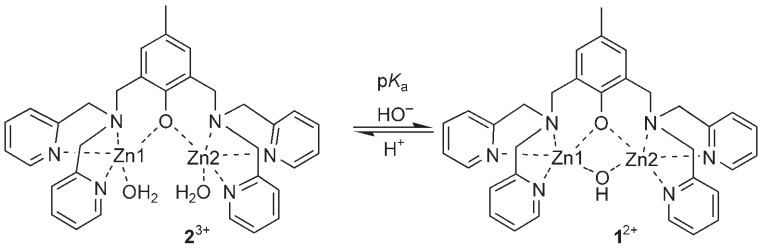

Scheme 2. pH-driven interconversion between $\mathbf{1}^{2+}$ and $\mathbf{2}^{3+}$.

at 25 °C. The reaction was monitored by following the increase in the absorbance observed at 400 nm (release of 4-nitrophenolate (PNPate)), as well as by ^{31}P NMR spectroscopy (formation of cycP, Scheme 1b). The reaction mixture was also analyzed by ESI-MS and no further hydrolysis of cycP was observed.

UV/Vis spectroscopic studies: The reaction was first performed in a mixture of H_2O/DMSO (70:30) without adjusting the pH. In the presence of excess substrate the cleavage reaction is catalyzed by **1**, but HPNP transesterification by **2** was not observed over the period of one week. To reveal the form of the active species in the HPNP transesterification reaction, a kinetic study was carried out by changing the pH of the 50 mM aqueous buffer/DMSO (70:30) solution at 25 °C. The dependence of the reaction rate of HPNP cleavage on pH in the presence of **1** and **2** is illustrated in Figure 3. The value of k_{obs} increased as the pH increased from 6.0 to 8.0 and then decreased slightly at higher pH values, which gave a sigmoidal curve for the cleavage reaction. Both complexes **1** and **2** gave the same k_{obs} values for all of the pH values. This behavior gives evidence for the interconversion of **2** into **1** and vice versa, which was already shown by ^{1}H NMR spectroscopy (see above). The data were fitted by the nonlinear least-squares method and gave a pH value of 7.40($\pm$0.02) at the inflection point, which is close to

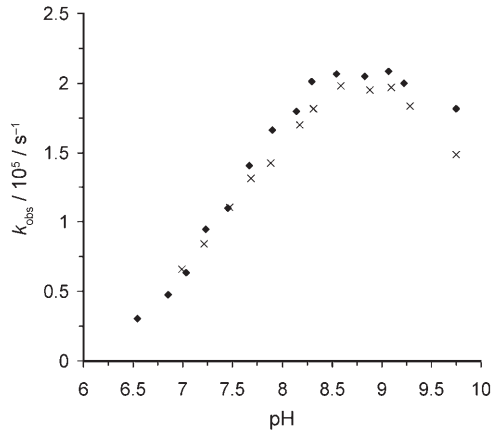

Figure 3. pH versus rate profile for the transesterification of HPNP (1 mM) catalyzed by **1** (◆, 0.5 mM) and **2** (×, 0.5 mM) in an aqueous mixture of buffer/DMSO (50 mM, 70:30) at 25 °C (MES: pH 5.5–6.5; HEPES: pH 7.0–8.2; CHES: pH 8.5–10.0).

the pK_a value of 7.60 obtained by the ^{1}H NMR spectroscopy titration. These observations suggest that the active species responsible for HPNP cleavage is **1** and in the following description of the detailed kinetic studies undertaken, it is only this complex in water/DMSO (70:30) without buffer or pH adjustment that will be presented.

The rate constant for the transesterification reaction (k_{obs}) shows a first-order dependence on the concentration of **1** at 25 °C (0.5–3 mM, Figure S3 in the Supporting Information). The second-order rate constant for **1** (k_{Zn}) determined from the slope of the graph is 3.8×10^{-2} M^{-1}s^{-1}. The initial rate of HPNP transesterification was also measured as a function of the substrate concentration (0.5–15 mM, Figure 4). At a

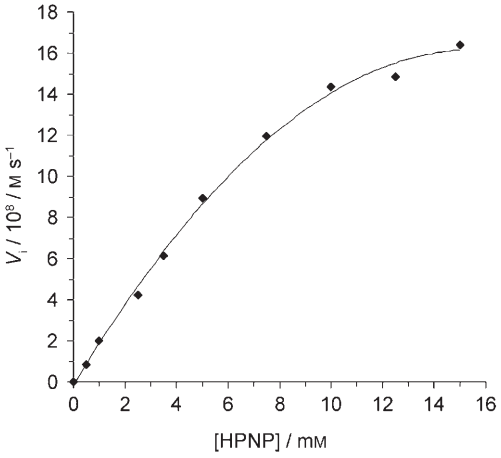

Figure 4. Saturation kinetics experiments for the transesterification of HPNP catalyzed by **1** (0.5 mM) in a mixture of water/DMSO (70:30) at 25 °C.

higher concentration of HPNP, saturation kinetics are observed, which implies that the cleavage reaction proceeds through a pre-equilibrium step between the complex and the substrate. The experimental data points are fitted to the Michaelis–Menten equation with $K_M = 13.5$ mM and $k_{cat} = 6.4 \times 10^{-4}\ s^{-1}$ determined from the Lineweaver–Burk double-reciprocal plot. The reciprocal of the Michaelis–Menten constant gives the substrate binding constant, $K_{ass} = 1/K_M = 74\ M^{-1}$. The uncatalyzed reaction of HPNP is relatively slow under these conditions ($k_{uncat} = 1.2 \times 10^{-8}\ s^{-1}$, half-life = 670 days).[16] However, in the presence of **1** (0.5 mM) the half-life decreases to 0.3 h, which means a $\approx 5.3 \times 10^4$-fold acceleration compared with HPNP autohydrolysis (k_{cat}/k_{uncat}). These values indicate a good catalytic activity and a moderate binding affinity of HPNP for **1**.[9]

Under the same conditions as those used for the catalysis in H_2O/DMSO (1.0 mM of HPNP and 0.5 mM of **1**) the reaction occurs rapidly in DMSO, which precludes the absorbance measurement and the determination of the reaction rate constant. Under dilute conditions the initial rate constant k_{obs} of this process is $6.85 \times 10^{-4}\ s^{-1}$ (0.1 mM of HPNP and 0.05 mM of **1** in DMSO), which corresponds to a ≈ 34-fold acceleration compared with HPNP hydrolysis in H_2O/DMSO ($k_{obs}^{DMSO}/k_{obs}^{H_2O/DMSO}$).

^1H and ^{31}P NMR spectroscopic studies: ^1H and ^{31}P NMR spectroscopy are suitable methods to study the binding of the phosphate diester and/or cycP to **1**. HPNP (1 or 5 equiv) was added to a solution of **1** in a mixture of D_2O/[D_6]DMSO (70:30). The ^1H NMR spectra showed new signals that were attributed to PNPate and cycP with concomitant high-field shifting and slight broadening of the complex signals (Figure S1b in the Supporting Information), which supports a symmetric bridging mode of the substrate on **1**. After hydrolysis of one equivalent of HPNP ($\delta_{HPNP} = -5.2$ ppm), the ^{31}P NMR spectrum showed only one signal shifted downfield ($\delta_1 = 18.4$ ppm) relative to an authentic cycP sample ($\delta_3 = 17.5$ ppm, Figure 5a and c). With five equivalents of HPNP, the signal ($\delta_2 = 17.9$ ppm) in the ^{31}P NMR spectrum was shifted upfield relative to δ_1 (Figure 5b). When authentic cycP (in its anionic form obtained from the barium salt) was added to the sample that contained **1** and HPNP (1 equiv), the slight shift from δ_1 to δ_2 was also observed, which provided evidence for the fast exchange between free and complexed cycP on the NMR spectroscopy timescale. These data suggest that cycP coordination to the dinuclear complex will remain symmetrical and consequently the OH bridge of **1** is preserved. We noted that the stereoisomers that result from the chiral cycP cannot be distinguished by NMR spectroscopy under the conditions of measurement.

In absolute [D_6]DMSO the addition of HPNP (1 equiv) induced drastic changes in the ^1H NMR spectrum of **1**. Two characteristic signals at $\delta = 1.9$ and 6.5 ppm that correspond to H_{methyl} and H_{phen} of the ligand BPMP were high-field shifted and split in two with other broad resonances of the Zn_2 complex, which indicated a strong modification of the complex structure and the presence of different species in solution (Figure S4b in the Supporting Information). This fact is supported by the ^{31}P NMR spectrum in which three signals are observed at $\delta_4 = 18.6$, $\delta_5 = 18.4$, and $\delta_6 = 17.1$ ppm (Figure 6a). When excess substrate was added, the signals at δ_4 and δ_5 disappeared, whereas a new signal at $\delta_7 = 14.3$ ppm that corresponds to the free cycP (Figure 6b) appeared. The two signals at δ_6 and δ_7 remained stable for weeks and on addition of further substrate only the proportion of free cycP increased.

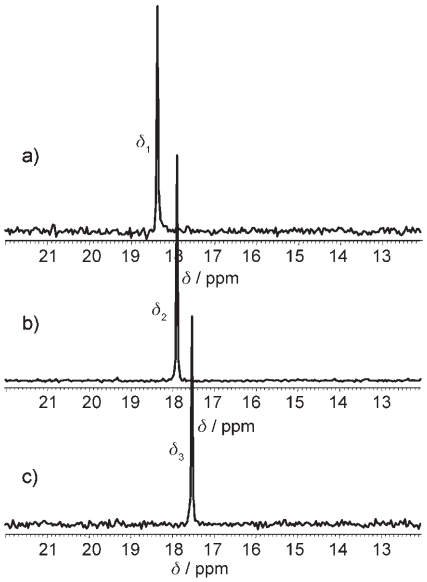

Figure 5. ^1H-decoupled ^{31}P NMR spectra of the reaction mixture in D_2O/[D_6]DMSO (70:30) after hydrolysis of a) 0.5 mM and b) 2.5 mM of HPNP by **1** (0.5 mM) at 25 °C, and c) an authentic cycP sample.

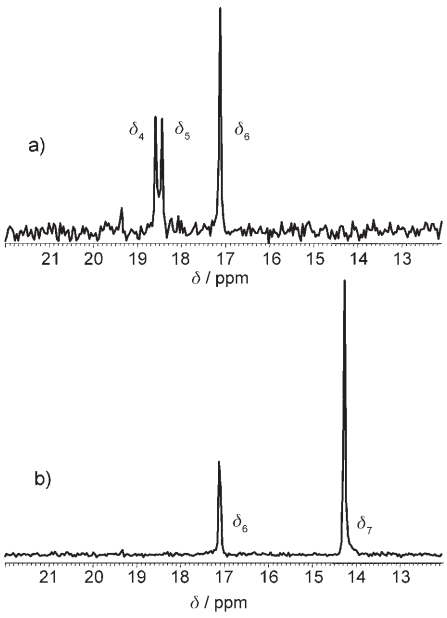

Figure 6. ^1H-decoupled ^{31}P NMR spectra of the reaction mixture in [D_6]DMSO after hydrolysis of a) 0.5 mM and b) 2.5 mM of HPNP by **1** (0.5 mM) at 25 °C.

With an excess of HPNP in [D_6]DMSO the ^{1}H NMR spectrum was simplified and only nine well-resolved signals that were attributed to the Zn_2 complex were present in the $\delta = 6$–9 ppm region (Figure 7). The resonances H_a–H_d were assigned to the protons of two pyridine rings by 2D COSY ^{1}H NMR spectroscopy at 25 °C. The triplet H_b shows cross-signals with both multiplet H_a and triplet H_c resonances, which allowed it to be ascribed to a β proton of the pyridine ring, and H_a and H_c were assigned as α- and γ-pyridine protons, respectively. The doublet H_d only displays a cross-peak with resonance H_c, and thus it was attributed to a δ-pyridine proton. Resonances H_1 to H_4 were assigned to the protons of two other pyridine rings, according to their relative integral intensity. The signal at $\delta = 6.4$ ppm corresponds to two H_{phen} protons. Two additional signals were observed at $\delta =$ 6.8 and 8.1 ppm (●) that correspond to PNPate in solution.

Further useful information could be obtained from the ^{1}H NMR spectrum in the $\delta = 1$–2 ppm region in which three resonances could be distinguished. The doublet at $\delta =$ 1.20 ppm (◇, $J = 6.14$ Hz) was assigned as the CH_3 protons of free cycP. The two doublet resonances at $\delta = 1.24$ and 1.28 ppm (♠, $J = 6.2$ and 6.1 Hz, respectively) integrated as three protons each relative to the three H_{methyl} protons of the BPMP ligand and were attributed to two CH_3 groups of two coordinated cycP units. The resonance of the H_{methyl} protons at $\delta = 1.89$ ppm is high-field shifted relative to **1**. These results suggest that the δ_6 signal in the ^{31}P NMR spectrum corresponds to a Zn_2 species in which two molecules of the product cycP are coordinated to the zinc ions. Furthermore, from an independent mixture of **1** and HPNP in a ratio of 1:3 in acetone and after diffusion of diethyl ether, we isolated the Zn_2 species with two coordinated cycP molecules as a powder (identified by the presence of the [Zn_2(bpmp)(cycP)$_2$]$^+$ ion in the ESI-MS and ^{31}P NMR spectra in [D_6]DMSO the observed signal is at $\delta = 17.05$ ppm, which was comparable with the signal at $\delta_6 = 17.1$ ppm in Figure 6). The ^{1}H NMR spectrum of this compound is shown in Figure S5 in the Supporting Information. Signals that correspond to complexed cycP form a multiplet, which results from the superposition of two sets of protons. These features support the hypothesis that there are two different coordination modes of cycP on the dinuclear zinc complex.

ESI-MS studies: The ESI-MS spectrum of the reaction solution that contain **1** (0.5 mM) and HPNP (0.5 mM, 1 equiv) in a mixture of H_2O/DMSO (70:30) showed two major signals at m/z 816 ($z = 1$) and 399 ($z = 2$) for [Zn_2(bpmp)(μ-OH)(cycP)]$^+$ and [Zn_2(bpmp)(cycP)]$^{2+}$, respectively, which corresponded to a complex in which the OH bridge is maintained with one molecule of cycP coordinated to the zinc ions (Figure S6 in the Supporting Information). Two additional signals were present at m/z 777 ($z = 1$) and 339 ($z = 2$) that corresponded to [Zn_2(bpmp)(μ-OH)(ClO_4)]$^+$ and [Zn_2(bpmp)(μ-OH)]$^{2+}$, respectively, which result from the initial Zn_2 complex (Figure S7 in the Supporting Information). When five equivalents of HPNP were added to the solution of **1** in H_2O/DMSO (70:30) after one day the ESI-MS spectrum showed two signals at m/z 880 ($z = 1$) and 399 ($z = 2$) that were attributed to [Zn_2(bpmp)(cycP)(CH_3COO) + Na]$^+$ and [Zn_2(bpmp)(cycP)]$^{2+}$, respectively (Figure S8).[17]

In absolute DMSO, the positively charged ESI-MS study of HPNP hydrolysis by **1** showed some similarities with previous experiments. In the presence of one equivalent of HPNP we observed signals from [Zn_2(bpmp)(cycP)(HCOO)]$^+$ and [Zn_2(bpmp)(cycP)]$^{2+}$ at m/z 843 ($z = 1$) and 399 ($z = 2$), respectively.[18] The signal from [Zn_2(bpmp)(μ-OH)]$^{2+}$ at m/z 339 ($z = 2$) resulted from the initial [Zn_2(bpmp)(μ-OH)(ClO_4)]$^+$ complex and the signal at m/z 935 ($z = 1$) for the [Zn_2(bpmp)(cycP)$_2$]$^+$ ion in which the Zn_2 complex that does not have an OH bridge coordinates to two cycP molecules were also detected (Figure S9 in the Supporting Information). In the presence of five equivalents of HPNP only one signal at m/z 935 ($z = 1$) for the [Zn_2(bpmp)(cycP)$_2$]$^+$ ion was observed. The ESI-MS spectra of all the species discussed are presented in Figures S6–S9 of the Supporting Information along with the corresponding theoretical isotopic patterns.

Theoretical results: We gained more information on the intermediates of both catalytic cycles from DFT calculations. To deal with such big systems, we used a newly developed approach that involves the Gaussian plane wave (GPW)[19] in CP2K-QuickStep[20] (see the Experimental Section). The main features of the calculated structure of $\mathbf{1}^{2+}$ are in good agreement with the results obtained by X-ray structural

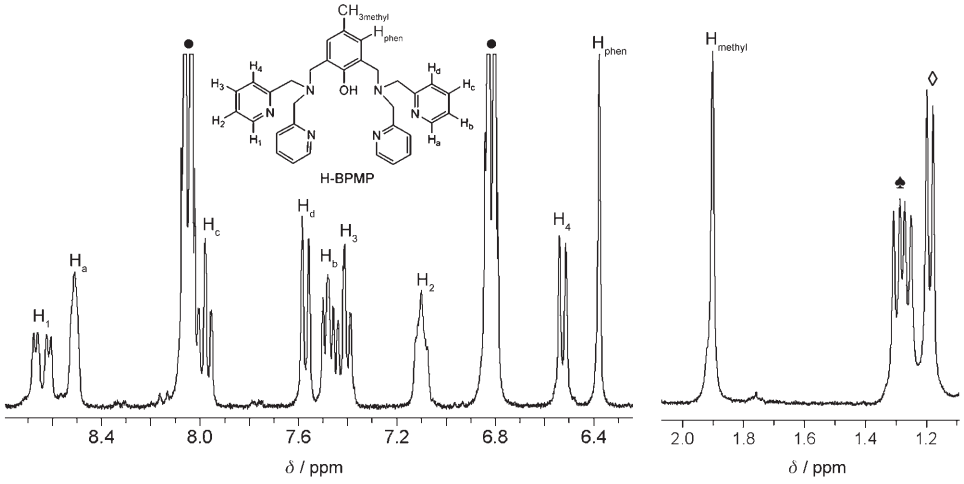

Figure 7. ^{1}H NMR spectrum of the reaction mixture in [D_6]DMSO after hydrolysis of HPNP (2.5 mM) by **1** (0.5 mM) at 25 °C. Labeled resonances correspond to PNPate (●), free cycP (◇), the Zn_2 species formed in the hydrolysis reaction according to the ligand scheme numbering, and to complexed cycP (♠).

analysis, which confirms the validity of the chosen level of theory (Table 1). First, we investigated the possible binding mode of HPNP to $\mathbf{1}^{2+}$. HPNP has three binding sites, the two oxygen atoms of the phosphoester unit and the hydroxy group on the alkyl arm. Therefore, the substrate can be coordinated to the dimetallic unit in various ways. We selected the more favorable binding mode[21] and the structure of $[Zn_2(bpmp)(\mu\text{-}OH)(hpnp)]^+$ (**VI**, Figure 8) seemed to be a

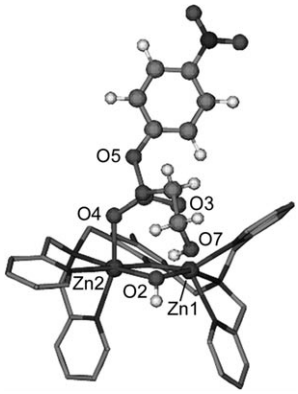

Figure 8. Calculated structure of $[Zn_2(bpmp)(\mu\text{-}OH)(hpnp)]^+$ (**VI**).

good starting point for the subsequent transesterification reaction. It presents a hydrogen bond between the hydroxy group of the HPNP ligand (O7) and the hydroxo bridge oxygen (O2) with also a weak interaction between O3 and Zn1 that leads to a highly asymmetric HPNP ligand with a Zn1–O3 distance of 2.79 Å versus a Zn2–O4 distance of 2.17 Å because of the steric hindrance between the HPNP substrate and the BPMP ligand (short nonbonding distances of the DFT-calculated structures are presented in Table 3). Highlighting the flexible role of the BPMP ligand, HPNP coordination induces structural rearrangement of the complex. Thus, the obtained structure **VI** presents a strongly distorted trigonal bipyramid geometry ($\tau = 0.66$) for Zn1, whereas Zn2 has a slightly distorted octahedral environment.

Table 3. Selected bond lengths [Å] of DFT-calculated structures.

	Zn1···Zn2	Zn1–O3	Zn2–O4	Zn1–O2 or Zn1–O3′	Zn2–O2 or Zn2–O3′
$\mathbf{1}^{2+}$	3.03	–	–	2.01	2.03
II	3.09	3.01	2.33	1.94	1.96
III	3.10	2.13	2.10	2.13	2.08
IV	3.08	2.19	2.08	2.10	2.04
V	3.18	2.63	2.14	2.08	2.08
VI	3.07	2.79	2.17	2.05	2.07
VII	3.38	2.08	2.09	3.52	2.34
VIII	3.43	2.13	2.21	3.39	2.22
IX	3.47	2.05	1.99	–	–
X	3.28	–	–	2.25	2.04
XI	3.13	2.64	2.11	2.10	2.22
XII	3.27	2.05	1.95	4.43	3.38
XIII	3.24	2.06	2.06	3.56	2.37

Next, we characterized the intermediates $[Zn_2(bpmp)(\mu\text{-}OH)(cycP)]^+$, $[Zn_2(bpmp)(cycP)]^{2+}$, and $[Zn_2(bpmp)(cycP)_2]^+$ that were revealed by NMR spectroscopy and ESI-MS measurements by means of DFT calculations (Figure 9). Complex $[Zn_2(bpmp)(\mu\text{-}OH)(cycP)]^+$ (**V**) shows

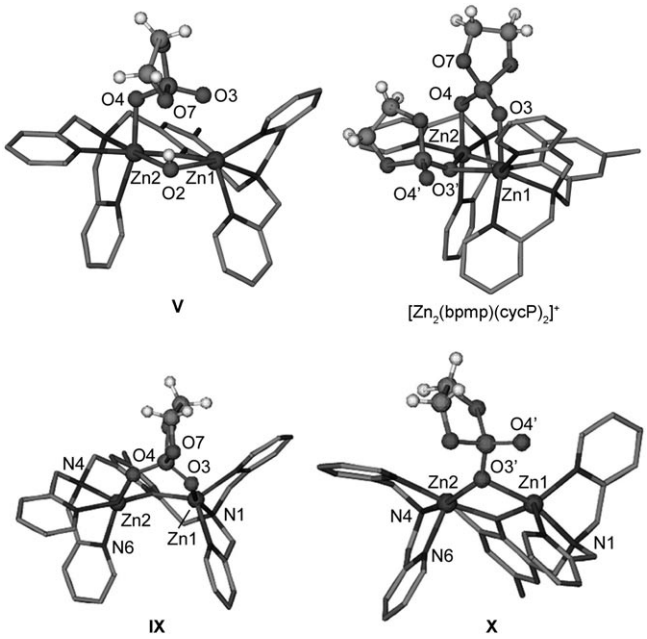

Figure 9. The calculated geometries of intermediates observed by ESI-MS.

a structure similar to **VI**, but with shorter Zn–O bonds (Zn1–O3 2.63 Å, Zn2–O4 2.14 Å, Table 3). For the $[Zn_2(bpmp)(cycP)]^{2+}$ complex, two different structures similar in energy have been found: $[Zn_2(bpmp)(\mu_{1,3}\text{-}cycP)]^{2+}$ (**IX**) with bidentate bridging ($\mu_{1,3}$) coordination of cycP and $[Zn_2(bpmp)(\mu_{1,1}\text{-}cycP)]^{2+}$ (**X**) with monodentate bridging ($\mu_{1,1}$) coordination. Bidentate structure **IX** is favored by 2 kcal mol^{-1} with quite a long intermetallic bond length (3.47 Å) and shorter Zn–O bond lengths (Zn1–O3 2.05 Å and Zn2–O4 1.99 Å) than the previous complexes (Table 3). Zn1 presents a distorted bipyramid trigonal environment with O3 and N1 in the axial positions ($\tau = 0.79$), whereas Zn2 has a square pyramidal environment with N4 in the apical position ($\tau = 0.28$). Only 2 kcal mol^{-1} higher in energy, monodentate complex **X** has a bipyramid trigonal environment for Zn1 ($\tau = 0.72$, with O3 and N1 still in axial positions) and a square pyramidal environment for Zn2 ($\tau = 0.16$ with N6 in the apical position instead of N4). We notice that the BPMP ligand arrangement is mostly the same for both complexes. Finally, the $[Zn_2(bpmp)(cycP)_2]^+$ intermediate revealed by ESI-MS in DMSO is structurally similar to **V**. Indeed, one of the cycP ligands is monodentate bridging ($\mu_{1,1}$) coordinated through the O3′ oxygen atom of the cycP (Zn1–O3′ 2.31 Å, Zn2–O3′ 2.12 Å), whereas the second one is bidentate bridging ($\mu_{1,3}$) coordinated (Zn1–O3 2.06 Å, Zn2–O4 2.06 Å).

Discussion

To investigate the zinc-containing RNase mechanism, dinuclear zinc model compounds **1** and **2** were studied as potential catalysts of HPNP transesterification. In a mixture of water/DMSO ^{1}H NMR spectroscopic studies revealed that **1** and **2** are reversibly interconverted upon acid/base titration (pK_a around 7.60, Scheme 2). The pH-dependence of the HPNP transesterification ability of **1** and **2** in the water/DMSO medium (pH optimal around 8–9, Figure 3) indicates that only complex **1** is suitable for HPNP hydrolysis. Moreover, to modulate the lypophilic/hydrophilic balance, the catalytic activity was studied under both aqueous (water/DMSO) and nonaqueous (DMSO) conditions. In all cases that involve excess HPNP, **1** shows multiple turnovers without loss of activity, which demonstrates that no product inhibition occurs during the catalytic cycle. The difference in reactivity between **1** and **2** can be explained by observing features of the catalytically active complex **1**. Complex **1** allows a bridging coordination of the substrate owing to a short Zn···Zn distance (3.016(1) in **1** vs. 3.791(1) Å in **2**), it also possesses an easily accessible metallic center (the change in coordination sphere from trigonal bipyramidal in **1** to square pyramidal in **2** increases the steric bulk around the zinc center), and it may involve the bound hydroxo as a general base. These requirements must play a major role in the catalysis, as already discussed by different groups for other series of complexes.[4,22]

Based on the UV/Vis, ^{1}H, and ^{31}P NMR spectroscopies, and ESI-MS analysis results, as well as on theoretical calculations, we next present and discuss the mechanisms of HPNP transesterification catalyzed by complex $\mathbf{1}^{2+}$ in aqueous (Scheme 3) and nonaqueous (Scheme 4) media.

Mechanism of transesterification in the aqueous medium: According to ESI-MS analysis, when one or more equivalents of substrate are added to **1** in aqueous solution, the dominant species are $\mathbf{1}^{2+}$ and **V** complexes. The presence of $\mathbf{1}^{2+}$ demonstrates that the OH bridge is stable or regenerated during the catalytic process. The absence of any complex formed between **1** and HPNP stresses the high reactivity of such an intermediate. The theoretical calculations led us to propose a substrate coordination mode (cf. the section on Theoretical results) and other plausible intermediates (Figure 10) in the catalytic cycle (Scheme 3).

A bidentate bridging coordination mode through two oxygen atoms of the phosphodiester group is proposed for the HPNP substrate and cycP product. This mode is supported by ^{1}H and ^{31}P NMR spectroscopy measurements that show high-field shifted ^{1}H NMR spectra relative to **1** with preservation of its symmetrical structure, and one downfield shifted phosphorus signal relative to an authentic cycP sample. This phosphodiester coordination mode has already been suggested or observed for some artificial dinuclear phosphodiesterases.[4,6,8,12,15,23–25]

As previously discussed, the hydroxypropyl arm in **VI** (Figure 8 and the section on Theoretical results) is oriented towards the OH bridge at a distance of 1.91 Å. This hydrogen bond facilitates substrate deprotonation by the hydroxo bridge. However, an explicit additional base is needed to generate experimentally revealed species **V**. We added a hydroxide anion in the proximity of $\mathbf{1}^{2+}$ that can contribute to the substrate deprotonation process (intermediate **II**).[26] Indeed, by capturing the bridging hydroxy proton, this exogenous base induces hydrogen-bond shortening (from 1.91 Å in **VI** to 1.61 Å in **II**) and the substrate can later be deprotonated through the OH bridge (Scheme 3).

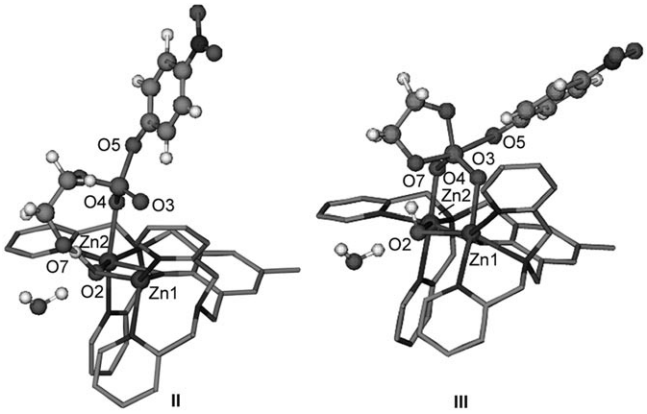

Figure 10. Calculated structures of intermediates in a mixture of H_2O/DMSO.

Afterwards, we investigated the intermediates of possible two-step mechanisms. First, the deprotonation of HPNP followed by P–O bond formation or vice versa; however, the formation of any intermediates could not be confirmed. Therefore, we assume that a concerted mechanism leads to the formation of intermediates with a pentacoordinated phosphorus atom (complexes **III** and **IV**, Scheme 3). In this **II**→**III** step, the BPMP ligand kept the same structure apart from an elongation of the Zn1–N2 length (from 2.12 Å in **II** to 2.40 Å in **III**) and this single modification allowed the ligand to adapt to the marked shortening of the Zn–O length (Zn1–O3 2.13 Å and Zn2–O4 2.10 Å, Table 3). Thus, the positively charged dinuclear center stabilizes and neutralizes the negative environment of the phosphorus atom more efficiently. To support this idea, calculations without the ligand BPMP have been performed and no stable pentacoordinated phosphorus intermediates were ever detected. In complex **III**, the pentacoordinated phosphorus atom exhibits trigonal bipyramid geometry with a long axial P–O bond length (P–O5 1.95 Å, P–O7 1.86 Å). The water molecule that is generated is kept within the complex environment through a hydrogen bond to the hydroxo bridge. This bond can be easily broken to lead to the formation of intermediate **IV**. The structural strain in compound **III** as a result of the hydrogen bond between O7 and the OH bridge is reduced in **IV** (O7–H 1.89 Å versus 1.72 Å in **III**), and the complex relaxes towards a more asymmetric structure in which the Zn1–O3 length is elongated (2.19 Å), whereas the Zn2–O4 length is shortened (2.08 Å, Table 3). Moreover, the new P–O7 bond is shortened (1.82 Å), whereas the

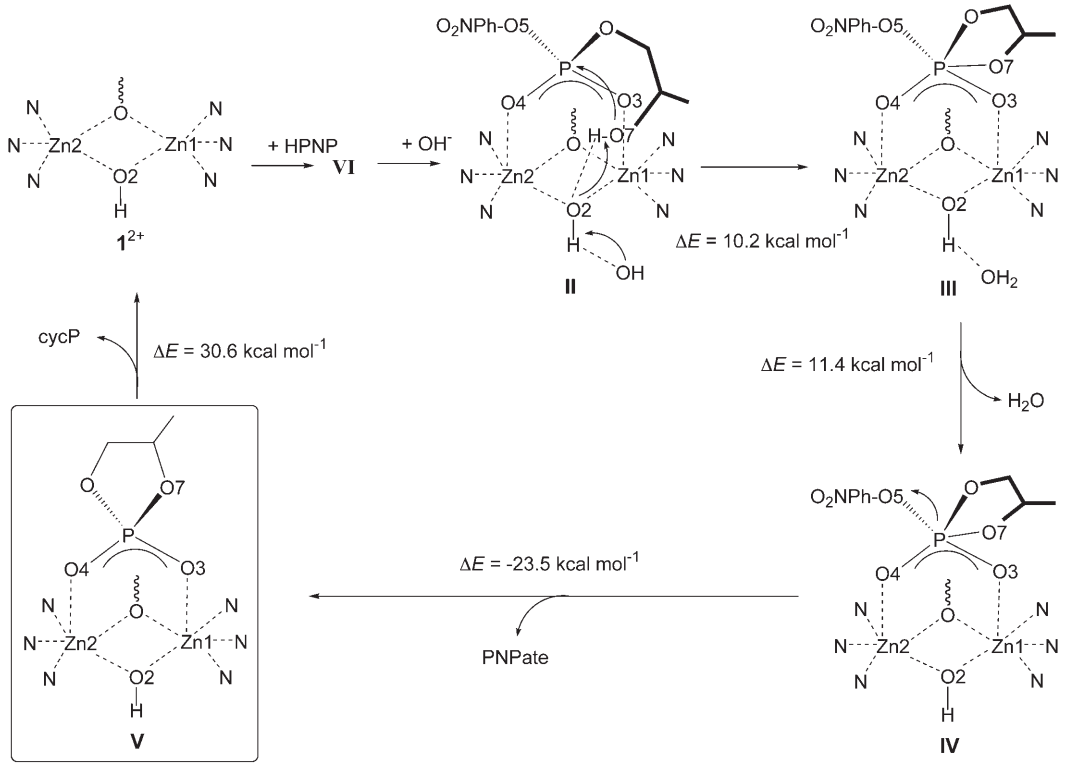

Scheme 3. Proposed mechanism for the HPNP transesterification reaction catalyzed by $\mathbf{1}^{2+}$ in H_2O/DMSO based on experimental data and DFT calculations. (Species **V** was characterized by ^{1}H and ^{31}P NMR spectroscopy and by ESI-MS analysis.)

breaking P–O5 bond lengthens (2.10 Å). In the last step, after the PNPate group leaves, compound **V** loses the cyclic phosphate and the initial $\mathbf{1}^{2+}$ complex is regenerated.

To conclude this section, the most striking facts about the mechanism of catalysis are the basic role of the hydroxo bridge/auxiliary base pair, and the stabilization of the pentacoordinated intermediates by the dizinc center associated with the flexibility of BPMP.

Mechanism of transesterification in the nonaqueous medium: In the nonaqueous medium, substrate deprotonation requires the bridging hydroxy to accept a proton, which leads to the destruction of the bridge (compound **VIII**, Figure 11) without any possible regeneration by an external base. Thus, this deprotonation step has to be considered as the first step of an initialization process that leads to the catalytic cycle. The mechanism proposed in Scheme 4 presents the initialization steps, compounds **VI** through to **IX**, and highlights the catalytic cycle itself, compounds **IX** to **XIII** (Figure 11).

The binding mode of HPNP (species **VI**) has already been discussed (see above). Deprotonation of the nucleophilic hydroxy moiety is concomitant with attack on the phosphorus atom, which leads to the formation of complex **VII**. However, in contrast with the aqueous media, the pentacoordinated phosphorus intermediate cannot be considered as viable and **VIII** is obtained by PNPate elimination from **VII**. This resulting complex presents a water molecule weakly bonded to the Zn2 atom (Zn2–O2 2.22 Å, Table 3). Zn1–O2 bond cleavage allows a strict trigonal bipyramid environment for Zn1 with N1 and O3 in the axial positions ($\tau = 0.99$). The elimination of this water molecule leads to the formation of **IX**, which is the first complex involved in the catalytic cycle.

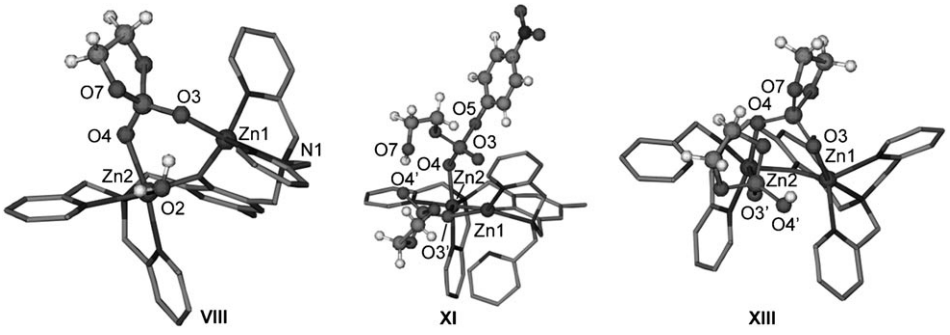

Figure 11. Calculated structures of intermediates in DMSO.

According to DFT calculations and evidence from NMR spectroscopy, the species $[Zn_2(bpmp)(cycP)]^{2+}$ presents two conformers in equilibrium, complex **IX** with a bidentate mode of coordination of cycP

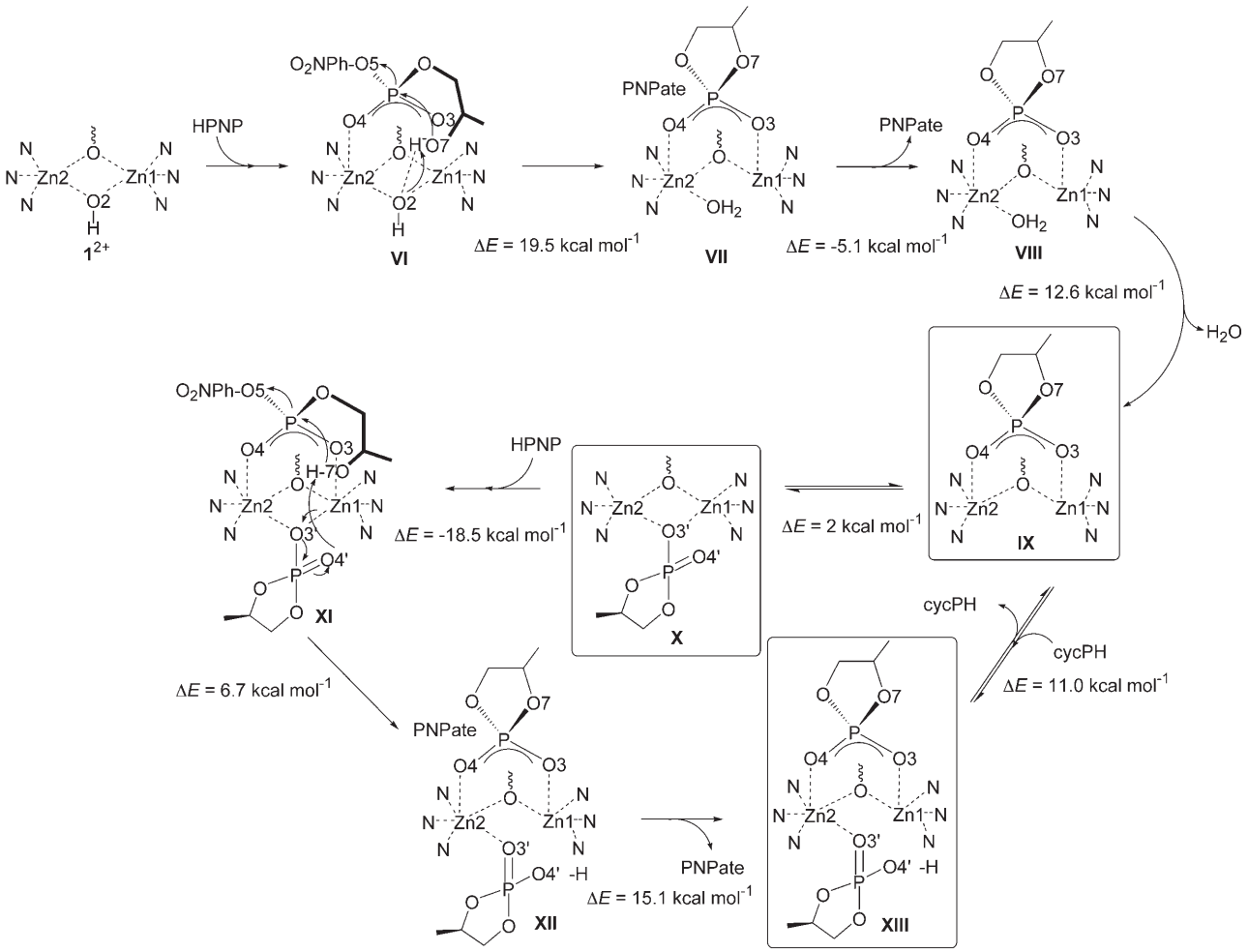

Scheme 4. Proposed mechanism for the HPNP transesterification reaction catalyzed by $\mathbf{1}^{2+}$ in DMSO based on experimental data and DFT calculations. (Species **IX**, **X**, and **XIII** were characterized by ^{1}H and ^{31}P NMR spectroscopy and by ESI-MS analysis.)

and complex **X** with a monodentate mode of coordination of cycP. Both the small energy difference of 2 kcal mol^{-1} and the absence of structural rearrangements strongly support the low activation energy for this bidentate/monodentate bridging mode equilibrium. This process is similar to the "carboxylate shift" already established from theoretical calculations and experiments on model compounds of zinc enzymes in which a carboxylate group close to the phosphate group can shift from monodentate bridging to other binding modes (monodentate terminal, bidentate chelating, and bidentate bridging) through a low-energy process.[27] To support this hypothesis, a temperature-dependent ^{31}P NMR spectroscopy measurement (between −10 and −40 °C in [D$_6$]acetone) was performed. After hydrolysis of HPNP (1 equiv), the ^{31}P NMR spectrum showed three signals (Figure 6) at room temperature, the signal at δ_6 was attributed to **XIII**,[28] and two other signals at δ_4 and δ_5 were attributed to the **IX** and **X** forms. The coalescence of the δ_4 and δ_5 signals at 40 °C clearly validates the presence of two species in equilibrium ($k_c = 27.2\ s^{-1}$ at 25 °C). With further decreases in temperature ([D$_6$]DMSO/[D$_6$]acetone) progressive decoalescence of the signals was observed until at −48 °C four signals are seen (Figure S10 in the Supporting Information). This behavior can be rationalized by exchange phenomenon, which includes the observation of isomers owing to chiral cycP. The monodentate bridging binding mode of phosphodiester to two metal ions similar to **X** has already been observed[24,29] or proposed.[22,30] But, to our knowledge, it is the first time that a "phosphate shift" has been brought to the fore in phosphate-containing zinc model compounds. The Zn2 ion in **IX** and **X** has square pyramidal coordination with a sixth available position (see above). However, if the substrate has no access to this sixth available position in **IX** owing to steric hindrance of the ligand, in complex **X** it can easily bind to Zn2 leading to intermediate **XI**. This compound is analogous to **VI** except that the hydroxo bridge is replaced by the P–O bridge of the cycP molecule. Similarly, the substrate hydroxypropyl arm is oriented towards the P–O4′ bond of the cycP at a distance of 1.96 Å. However, complex **XI** exhibits a more reactive structure than **VI**, which is its hydroxo bridge analogue owing to a stronger Lewis acid activation through shorter Zn–O bonds (Zn1–O3 2.64 Å in **XI** versus 2.79 Å in **VI** and Zn2–O4 2.11 Å in **XI** versus 2.17 Å in **VI**, Table 3) and a

better conformation for P–O7 bond formation (P–O7 3.68 Å in **XI** versus 3.74 Å in **VI**). Then, complex **XI** undergoes transesterification to form **XII** the same way as **VI** did during the initialization stage. In fact, no pentacoordinated phosphorus species between **XI** and **XII** were revealed by theoretical calculations, in the same manner as between **VI** and **VII**. Next, PNPate elimination yields **XIII** in which cycP protonation induces elongation of the Zn1–O3′ (3.56 Å) and Zn2–O3′ (2.37 Å) bonds to favor product release (Table 3). To give an account of the multiple turnovers, we assume that there is an equilibrium between complex **XIII** and species **IX** and **X**. In the presence of an excess of cycP, this equilibrium would be shifted towards **XIII**. The ^{31}P NMR spectroscopy measurements support this hypothesis: after the hydrolysis of HPNP (1 equiv), we detected **XIII** in a ratio of 1:3 relative to **IX** and **X**, but after the addition of an excess of cycP, this ratio increases. Note that after the hydrolysis of HPNP (1 equiv), we also identified $\mathbf{1}^{2+}$ (ESI-MS) and the fact that **X** reacts faster with the substrate than complex $\mathbf{1}^{2+}$. Moreover, upon addition of HPNP to **XIII**, the catalytic cycle restarts until the hydrolysis of the substrate is complete. To the best of our knowledge, the only example of two cycP molecules coordinated to a dimetallic center was published by Tsang et al.[25] Two cycP molecules were coordinated in a bidentate bridging mode to two La^{3+} ions. However, it is the first bidentate bridge with a monodentate bridging coordination mode proposed.

In conclusion, for a DMSO medium, we have proposed a novel type of mechanism for the transesterification reaction. The first step corresponds to OH bridge destruction and the second step is a cycle in which diphosphate complexes are the key intermediates.

Comparison of the two mechanisms in the different media: Previous work (without transition metals) published in the literature has revealed a significant acceleration of the rate of alkaline hydrolysis of different mono- or diester phosphates in aqueous solution on addition of dipolar solvents, such as DMSO.[31] The level of DMSO can reach 98%. The most striking experimental fact from our results is probably the speed and efficiency of the catalyzed transesterification reaction in pure DMSO compared with in the DMSO/aqueous medium. An explanation can be obtained from the comparison of the two corresponding mechanisms. First, let us compare the key step of these reactions, the P–O bond formation, that is, the **II**→**III** step (Scheme 3) in aqueous medium and the **XI**→**XII** step (Scheme 4) in DMSO.[32] The thermodynamic cost is clearly more favorable in DMSO than in the aqueous medium, 6.7 versus 10.2 kcal mol^{-1}. So, the key step should be faster in the mechanism proposed for the DMSO medium. Another limiting step that we can focus on is the product-release step. Once more, the proposed mechanisms favor faster kinetics in DMSO from a thermodynamic point of view (11.0 kcal mol^{-1} between **XIII** and **IX** (Scheme 4) versus 30.6 kcal mol^{-1} between **V** and $\mathbf{1}^{2+}$ (Scheme 3)). Finally, the major difference is the role of the bridge as a base and its eventual regeneration. In the aqueous medium case, the OH bridge acts as a relay base, and consequently, a basic medium is needed to regenerate it. Thus, the role of the OH bridge is not only structural; its importance is as a result of its role as a relay base. This hypothesis is confirmed by the fact that fixation of the substrate is detected by ^{31}P NMR spectroscopy of **2** despite its lack of reactivity. In the organic medium, to enter the cycle from **IX** to **XIII**, destruction of the OH bridge is required and it is replaced by a phosphate bridge that allows the phosphate to play the role of proton acceptor. Thus, the cycle runs thanks only to the phosphate that replaces OH/water in the role of relay base. The mechanism of Scheme 4 is not observed in an aqueous medium according to data obtained by NMR spectroscopy because the characteristic complexes with two phosphates were not detected. The passage from complex **VIII** to complex **IX** concomitant with the release of water seems unlikely in a water medium. The mechanism in the DMSO medium (which does not need a basic medium) is very efficient thanks to the substrate. This pathway is clearly a good candidate for explaining the mechanism in the buried active sites found in enzymes.

Conclusion

A detailed hydrolytic activity study has been carried out on two dizinc model systems (**1** and **2**) that undergo pH-driven interconversion. Hydrolysis of HPNP as a substrate model for RNA was promoted by **1**, but no activity was observed over one week with **2** despite the fixation of the substrate, as shown by ^{31}P NMR spectroscopy. These results give direct experimental evidence of the requirements of the transesterification reaction, which are Zn···Zn separation, accessibility of the substrate, and a hydroxo ligand bound to zinc.

Complex **1** has good activity that is considerably enhanced compared with the spontaneous hydrolysis rate (10^4 in water/DMSO (70:30)), and multiple turnover without significant loss of activity, which demonstrates that no product inhibition occurred during the catalytic cycle. According to the catalytic conditions (nonaqueous and aqueous/DMSO), complex **1** exhibits different behavior. The synergistic interdisciplinary approach used herein allowed the substrate/product-binding mode on the dinuclear dizinc core to be discerned along with the role and the identity of the key species involved. In the mixed aqueous/DMSO medium, complex **1** undergoes multiple turnover and retains its initial double-bridged structure. The presence of an additional hydroxide ion from the solvent helps substrate deprotonation. The pentacoordinated phosphorus intermediate **IV** is stabilized by the short Zn···Zn distance (3.08 Å). The cyclic phosphate product is reversibly coordinated to the complex and substituted by the substrate upon addition of excess substrate. In the organic medium, the mechanistic scenario starts in the same way, but without regeneration of the OH bridge. Five consecutive intermediates (**IX**–**XIII**) were calculated for the catalytic cycle. The equilibrium between **IX** and **X** provides evidence for the two bridging modes of the

cyclic phosphate. The presence of additional substrate led to the formation of **XIII**, which has two cyclic phosphates coordinated in an unusual way.

The bridging OH group available in **1** plays a key role in the aqueous medium as a relay base, which emphasizes the need for a basic medium. On the other hand, the OH bridge is replaced by the substrate itself as a proton acceptor in the nonaqueous medium.

For this important transesterification reaction, our results show that multiple viable catalytic strategies are to be considered that depend on the hydrophilic/lipophilic balance in the local environment of the active site. This improved understanding of the mechanism will assist the engineering of artificial hydrolases.

Experimental Section

General information: NMR spectra (^{1}H and ^{31}P) were recorded by using a Bruker Avance 300 spectrometer at 300 MHz for ^{1}H and at 121.5 MHz for ^{31}P. Chemical shifts are reported in ppm, and for ^{1}H NMR spectra, chemical shifts were referenced to the solvent signal, and for ^{31}P NMR spectra, 85% phosphoric acid was used as the external reference. The IR spectra were recorded by using a Nicolet Magna-IR 550 spectrometer. Electrospray mass spectra were recorded by using an Esquire 3000 plus Bruker Daltonics and/or Quattro LCZ Waters-Micromass instrument with a nanospray inlet. Solution pHs were measured at 25 °C with a Metrohm 713 pH meter equipped with a Metrohm combined LL micro pH glass electrode that was calibrated with standard pH buffer solutions. Kinetic measurements were recorded by using a quartz cuvette (1.0 cm) and a Varian Cary 50 UV-Visible spectrophotometer equipped with a Peltier thermostatting accessory.

Materials: The preparation of H-BPMP has been described previously.[33] The RNA model substrates HPNP and cycP were synthesized according to previously described procedures.[34] Commercially available DMSO was freshly distilled and stored over molecular sieves (3 Å). Other commercial starting materials and solvents were of analytical grade and were used without further purification.

Caution! Although no problems were encountered, suitable care and precautions should be taken when handling perchlorate salts.

Complex 1: A solution of $Zn(ClO_4)_2{\cdot}6H_2O$ (211 mg, 0.56 mmol) in CH_3CN (5 mL) was added dropwise to H-BPMP (150 mg, 0.28 mmol) dissolved in CH_3CN (5 mL) and the mixture was stirred for 10 min at room temperature. NEt_3 (80 mL, 0.57 mmol) was then added and the solution was stirred for another 30 min at room temperature. The solvent was partially removed under reduced pressure and the resulting solution (7 mL) was allowed to stand overnight at −20 °C. The white powder that formed was collected by filtration and colorless crystals that were suitable for X-ray diffraction were obtained by slow vapor diffusion of THF into a saturated solution of **1** in CH_3CN at −20 °C. ^{1}H NMR (300 MHz, [D$_6$]DMSO, 25 °C): $\delta = 2.04$ (s, 3H), 3.55–3.65 (m, 4H), 3.97–4.10 (m, 8H), 6.71 (s, 2H), 7.56–7.59 (m, 4H), 7.62–7.67 (m, 4H), 8.06 (td, J(H,H) = 6.0 Hz and J(H,H) = 1.7 Hz, 4H), 8.90 ppm (d, J(H,H) = 4.7 Hz, 4H); IR (KBr): $\tilde{\nu} = 1608$ (C=N py), 1480, 1440 (C−C py), 1082, 621 cm^{-1} (ClO_4); MS (ESI, CH_3CN): m/z: 777 ($z = 1$, $[Zn_2(bpmp)(\mu\text{-}OH)(ClO_4)]^+$), 339 ($z = 2$, $[Zn_2(bpmp)(\mu\text{-}OH)]^{2+}$); elemental analysis calcd (%) for $C_{33}H_{34}N_6O_2Zn_2{\cdot}2ClO_4{\cdot}0.5C_4H_8O$ (**1**·0.5C_4H_8O) (911.8): C 46.06, H 4.16, N 9.21; found: C 46.10, H 4.28; N 9.19.

Complex 2: A solution of $Zn(ClO_4)_2{\cdot}6H_2O$ (281 mg, 0.754 mmol) in water (3 mL) was added dropwise to H-BPMP (200 mg, 0.377 mmol) dissolved in acetone (5 mL) and the mixture was stirred for 30 min at room temperature. The solvent was partially removed under reduced pressure and the resulting solution was allowed to stand overnight at +4 °C. The white powder that formed was collected by filtration and was recrystallized from hot water. ^{1}H NMR (300 MHz, [D$_6$]acetone, 25 °C): $\delta = 1.83$ (s, 3H), 3.65 and 4.44 (d, J^{AB}(H,H) = 12.3 Hz, 4H), 3.98 and 4.12 (d, J^{AB}(H,H) = 16.9 Hz, 4H), 4.45 and 4.62 (d, J^{AB}(H,H) = 17.2 Hz, 4H), 6.63 (s, 2H), 7.05 (m, 2H), 7.24 (m, 2H), 7.67 (m, 6H), 8.12 (m, 2H), 8.48 and 8.80 ppm (d, J^{AB}(H,H) = 5.1 Hz, 4H); IR (KBr): $\tilde{\nu} = 1609$ (C=N py), 1485, 1440 (C−C py), 1070, 621 cm^{-1} (ClO_4); elemental analysis calcd (%) for $C_{33}H_{37}N_6O_3Zn_2{\cdot}3ClO_4{\cdot}4H_2O$ (**2**·4H_2O) (1066.87): C 37.14, H 4.22, N 7.87; found: C 37.30, H 4.30, N 7.69.

^{1}H NMR spectroscopic titration: The protonation constant of zinc-coordinated water was determined by ^{1}H NMR spectroscopy. Samples of **1** and **2** (5 mM) were prepared in D_2O/[D$_6$]DMSO (70:30) and were used for the pD NMR spectroscopy titration. The pD (pD = pH + 0.4)[35] of the solution was adjusted with DCl and NaOD solutions. The pH value obtained corresponds to the reading on the pH meter, which was previously calibrated with standard aqueous buffers. All pH-dependent NMR spectroscopy measurements were performed at 25 °C.

Kinetics: The rate of the HPNP transesterification reaction catalyzed by **1** and **2** was measured spectrophotometrically by monitoring the production of PNPate at 400 nm ($\varepsilon = 18500$ dm^3 mol^{-1} cm^{-1}) in a mixture of 50 mM buffer (0.1 M $NaClO_4$)/DMSO (70:30). The extinction coefficient of PNPate in DMSO at $\lambda_{max} = 440$ nm is $\varepsilon = 22500$ dm^3 mol^{-1} cm^{-1}. Typically, the reaction was initiated by injecting a concentrated solution of HPNP (15 μL, 0.168 M in H_2O, final concentration 1.0 mM) into a solution of zinc complex (2.5 mL, 0.5 mM) maintained at 25 °C. The solution of zinc complex was buffered with MES (pH 5.5–6.5), HEPES (pH 7.0–8.2), and CHES (pH 8.5–10), and the ionic strength was maintained with 0.1 M $NaClO_4$. The first-order rate constants (k_{obs}, s^{-1}) of the HPNP transesterification reaction catalyzed by the two zinc complexes were calculated by the initial rate method. The absorbance was converted into concentration by using Equations (1; with O.D. as optical density) to (3) and the initial reaction rate (V_i, M s^{-1}) was calculated from the plots of $[PNPate]_{total}$ versus time. V_i divided by the concentration of HPNP gives k_{obs}. The pK_a of 4-nitrophenol (PNP) at 25 °C was determined under these conditions to be 7.15; this value was used to correct the degree of ionized PNP at different pH values.

$$[PNPate]_{measured} = \frac{O.D.}{\varepsilon_{400nm}} \quad (1)$$

$$pH\ 7.15 + \log \frac{[PNPate]_{measured}}{[PNP]} \quad (2)$$

$$[PNPate]_{total} = [PNPate]_{measured} + [PNP] \quad (3)$$

Computational details: The quantum chemical calculations were performed by using the CP2K-QuickStep[20] program at the DFT level with the BLYP[36] functional. QuickStep is an implementation of the GPW[19] method that is based on the Kohn–Sham formulation of DFT. It is a hybrid method that uses a linear combination of Gaussian-type orbitals to describe the Kohn–Sham orbitals, whereas an auxiliary plane waves basis set is employed to expand the electronic charge density. The basis set used was a double-zeta valence set of Gaussian orbitals[32] with a polarization set added for all atoms in conjunction with the Goedecker–Teter–Hutter[37] pseudopotentials also for all atoms. The auxiliary PW basis set was defined by a cubic box of (18 Å)^3 and by a density cut off of 300 Ry for the larger grid. Geometry optimizations were performed on the entire system, except for the methyl group of HPNP (and cycP) which was replaced by an hydrogen atom to limit the number of possible intermediates. Cartesian coordinates for all of the calculated structures are presented in the Supporting Information.

Crystallography: Crystals were mounted on a Bruker AXS-Enraf-Nonius Kappa CCD diffractometer equipped with graphite-monochromated $Mo_{K\alpha}$ radiation ($\lambda = 0.71073$ Å) and a cryostream cooler. For both compounds reflections were collected and corrected for Lorentzian and polarization effects. Structures were solved by direct methods with the use of the SIR92[38] software and refined by using the TeXsan[39] program package. All non-hydrogen atoms were refined with anisotropic thermal parameters. Hydrogen atoms were generated at idealized positions, or by

using the Fourier difference, riding on the carrier atoms with isotropic thermal parameters.

Crystal data for ***1***·*THF*·*0.67CH$_3$CN*·*0.33H$_2$O*:[40] Formula = $C_{38.33}H_{44.67}N_{6.67}O_{11.33}Cl_2Zn_2$; $M_w = 981.10$; monoclinic; space group $P21/c$; colorless block ($0.32 \times 0.23 \times 0.22$ mm); $a = 20.576(2)$, $b = 9.9097(8)$, $c = 24.051(3)$ Å; $\beta = 103.550(9)°$; $V = 4767.5(8)$ Å^3; $Z = 4$; $\rho_{calcd} = 1.359$ g cm^{-3}; $T = 150$ K; $\mu(Mo_{K\alpha}) = 1.178$ mm^{-1}. A total of 36743 reflections were collected. Final refinement with 649 variables led to $R = 0.0647$ (for 6672 reflections, $F = 2\sigma(F)$), $R_w = 0.0925$, goodness of fit $S = 1.70$, max/min residual peaks = 1.48/−1.21 e Å^{-3}.

Crystal data for ***2***·*4H$_2$O*: Formula = $C_{33}H_{45}N_6O_{19}Cl_3Zn_2$; $M_w = 1066.87$; orthorhombic; space group *Pbcn*; colorless block ($0.25 \times 0.20 \times 0.18$ mm); $a = 16.193(1)$, $b = 16.527(1)$, $c = 16.673(1)$ Å; $V = 4462.1(4)$ Å^3; $Z = 4$; $\rho_{calcd} = 1.588$ g cm^{-3}; $T = 293$ K; $\mu(Mo_{K\alpha}) = 1.335$ mm^{-1}. A total of 52347 reflections were collected. Final refinement with 287 variables led to $R = 0.0448$ (for 2490 reflections, $F = 2\sigma(F)$), $R_w = 0.0562$, goodness of fit $S = 1.51$, max/min residual peaks = 0.53/−0.49 e Å^{-3}.

CCDC-619206 for **1** and CCDC-293669 for **2** contain the supplementary crystallographic data for this paper. These data can be obtained free of charge from The Cambridge Crystallographic Data Centre via www.ccdc.cam.ac.uk/data_request/cif.

Acknowledgements

The authors thank Dr. Pierre Vatton and Régis Gras (DCM) for their technical help, Sylvette Beyne (DCM) for her assistance with the variable-temperature ^{31}P NMR spectroscopy measurements, and Dr. Heinrich Luftmann (Münster) for measuring some of the ESI-MS spectra. The Université Joseph Fourier (UJF) and the center CECIC are also acknowledged for providing computer facilities. This work was supported by a joint CNRS/DFG program "Learning from nature how two-metal centers operate: studies of purple acid phosphatases (PAP) and polyphenol oxidases (PPO)—enzymes and models" with a grant for K.S. Financial support from the UJF/CNRS (UMR 5616 and FR 2607) and from the Ministère de l'Education (C.M.) are also gratefully acknowledged.

[1] J. F. Davies, Z. Hostomska, S. R. Jordan, D. Matthews, *Science* **1991**, *252*, 88–95.
[2] A. Lahm, A. Voldeba, D. J. Suck, *J. Mol. Biol.* **1990**, *215*, 207–210.
[3] a) J. E. Bacher, W. Kauzmann, *J. Am. Chem. Soc.* **1952**, *74*, 3779–3786; b) D. Lipkin, P. T. Talbert, M. Cohn, *J. Am. Chem. Soc.* **1954**, *76*, 2871–2872; c) D. M. Brown, D. I. Magrath, A. H. Neilson, A. R. Todd, *Nature* **1956**, *177*, 1124–1125.
[4] a) K. Worm, F. Chu, K. Matsumoto, M. D. Best, V. Lynch, E. V. Anslyn, *Chem. Eur. J.* **2003**, *9*, 741–747; b) B. Bauer-Siebenlist, F. Meyer, E. Farkas, D. Vidovic, S. Dechert, *Chem. Eur. J.* **2005**, *11*, 4349–4360.
[5] a) A. O'Donoghue, S. Y. Pyun, M.-Y. Yang, J. R. Morrow, J. P. Richard, *J. Am. Chem. Soc.* **2006**, *128*, 1615–1621; b) O. Iranzo, A. Y. Kovalevsky, J. R. Morrow, J. P. Richard, *J. Am. Chem. Soc.* **2003**, *125*, 1988–1993; c) J. G. Zalatan, D. Herschlag, *J. Am. Chem. Soc.* **2006**, *128*, 1293–1303; d) P. Rossi, F. Felluga, P. Tecilla, F. Formaggio, M. Crisma, C. Toniolo, P. Scrimin, *J. Am. Chem. Soc.* **1999**, *121*, 6948–6949.
[6] O. Iranzo, T. Elmer, J. P. Richard, J. R. Morrow, *Inorg. Chem.* **2003**, *42*, 7737–7746.
[7] a) J. Weston, *Chem. Rev.* **2005**, *105*, 2151–2174; b) N. Sträter, W. N. Lipscomb, T. Klabunde, B. Krebs, *Angew. Chem.* **1996**, *108*, 2158–2191; *Angew. Chem. Int. Ed. Engl.* **1996**, *35*, 2024–2055; c) D. E. Wilcox, *Chem. Rev.* **1996**, *96*, 2435–2458; d) D. M. Perreault, E. V. Anslyn, *Angew. Chem.* **1997**, *109*, 470–490; *Angew. Chem. Int. Ed. Engl.* **1997**, *36*, 432–450.
[8] E. Kimura, *Curr. Opin. Chem. Biol.* **2000**, *4*, 207–213.
[9] J. R. Morrow, O. Iranzo, *Curr. Opin. Chem. Biol.* **2004**, *8*, 192–200.
[10] N. H. Williams, B. Takasaki, M. Wall, J. Chin, *Acc. Chem. Res.* **1999**, *32*, 485–493.
[11] A. W. Addison, T. N. Rao, J. Reedijk, J. van Rijn, G. C. Verschoor, *J. Chem. Soc., Dalton Trans.* **1984**, 1349–1356.
[12] a) J. Chen, X. Wand, Y. Zhu, J. Lin, X. Yang, Y. Li, Y. Lu, Z. Guo, *Inorg. Chem.* **2005**, *44*, 3422–3430; b) S. Albedyhl, D. Schnieders, A. Jancsó, T. Gajda, B. Krebs, *Eur. J. Inorg. Chem.* **2002**, 1400–1409.
[13] a) S. Uhlenbrock, B. Krebs, *Angew. Chem.* **1992**, *104*, 1631–1632; *Angew. Chem. Int. Ed. Engl.* **1992**, *31*, 1647–1648; b) H. Carlson, M. Haukka, E. Nordlander, *Inorg. Chem.* **2004**, *43*, 5681–5687.
[14] G. Schwarzenbach, K. Schwarzenbach, *Helv. Chim. Acta* **1963**, *46*, 1390–1400.
[15] B. Bauer-Siebenlist, F. Meyer, E. Farkas, D. Vidovic, J. A. Cuesta-Seijo, R. Herbst-Irmer, H. Pritzkow, *Inorg. Chem.* **2004**, *43*, 4189–4202.
[16] I. O. Fritsky, R. Ott, H. Pritzkow, R. Krämer, *Chem. Eur. J.* **2001**, *7*, 1221–1231.
[17] In the former complex the OH bridge was probably substituted by CH_3COO^- present in the MS machine.
[18] In the former complex the OH bridge was probably substituted by $HCOO^-$ present in the MS machine.
[19] G. Lippert, J. Hutter, M. Parrinello, *Mol. Phys.* **1997**, *92*, 477.
[20] J. VandeVondele, M. Krack, F. Mohamed, M. Parrinello, T. Chassaing, J. Hutter, *Comput. Phys. Commun.* **2005**, *167*, 103–128.
[21] This structure is only 0.3 kcal mol^{-1} higher in energy than the most stable structure found. Nevertheless it exhibits coordination of the HPNP ligand to the zinc atoms as well as coordination of the hydroxy group, which prevents this structure from being reactive.
[22] W. H. Chapman, R. Breslow, *J. Am. Chem. Soc.* **1995**, *117*, 5462–5469.
[23] a) M. Yashiro, H. Kaneiwa, K. Onaka, M. Komiyama, *Dalton Trans.* **2004**, 605–610; b) D. Wahnon, A.-M. Lebuis, J. Chin, *Angew. Chem.* **1995**, *107*, 2594–2597; *Angew. Chem. Int. Ed. Engl.* **1995**, *34*, 2412–2414; c) N. H. Williams, A.-M. Lebuis, J. Chin, *J. Am. Chem. Soc.* **1999**, *121*, 3341–3348; d) F. Mancin, E. Rampazzo, P. Tecilla, U. Tonellato, *Eur. J. Org. Chem.* **2004**, 281–288; e) R. Jikido, H. Shiraishi, K. Matsufuji, M. Ohba, H. Furutachi, M. Suzuki, H. Okawa, *Bull. Chem. Soc. Jpn.* **2005**, *78*, 1795–1803; f) C. Bazzicalupi, A. Bencini, E. Berni, A. Bianchi, P. Fornasari, C. Giorgi, B. Valtancoli, *Inorg. Chem.* **2004**, *43*, 6255–6265; g) E. Stulz, H. B. Bürgi, C. Leumann, *Chem. Eur. J.* **2000**, *6*, 523–536; h) S. Albedyhl, M. T. Averbuch-Pouchot, C. Belle, B. Krebs, J. L. Pierre, E. Saint-Aman, S. Torelli, *Eur. J. Inorg. Chem.* **2001**, 1457–1464; i) T. Gajda, R. Krämer, A. Jancsó, *Eur. J. Inorg. Chem.* **2000**, 1635–1644; j) N. V. Kaminskaia, C. He, S. J. Lippard, *Inorg. Chem.* **2000**, *39*, 3365–3373; k) P. Molenveld, J. F. J. Engbersen, H. Kooijman, A. L. Spek, D. N. Reinhoudt, *J. Am. Chem. Soc.* **1998**, *120*, 6726–6737; l) J. Chin, *Curr. Opin. Chem. Biol.* **1997**, *1*, 514–521; m) M. Yashiro, R. Kawahara, *J. Biol. Inorg. Chem.* **2004**, *9*, 914–921; n) A. Bencini, E. Berni, A. Bianchi, V. Fedi, C. Giorgi, P. Paoletti, B. Valtancoli, *Inorg. Chem.* **1999**, *38*, 6323–6325; o) O. Iranzo, J. P. Richard, J. R. Morrow, *Inorg. Chem.* **2004**, *43*, 1743–1750.
[24] C. He, S. J. Lippard, *J. Am. Chem. Soc.* **2000**, *122*, 184–185.
[25] J. S. W. Tsang, A. A. Neverov, R. S. Brown, *J. Am. Chem. Soc.* **2003**, *125*, 1559–1566.
[26] This additional hydroxide ion can be considered as a model for any base present in the medium.
[27] a) R. L. Rardin, W. B. Tolman, S. J. Lippard, *New J. Chem.* **1991**, *15*, 417–430; b) A. Demsar, J. Kosmrlj, S. Petricek, *J. Am. Chem. Soc.* **2002**, *124*, 3951–3958; c) B.-H. Ye, X.-Y. Li, I. D. Williams, X.-M. Chen, *Inorg. Chem.* **2002**, *41*, 6426–6431; d) X.-M. Chen, Y.-X. Tong, T. C. W. Mak, *Inorg. Chem.* **1994**, *33*, 4586–4588.
[28] Variable-temperature ^{31}P NMR spectroscopy measurements support the presence of two different coordinated phosphates in **XIII**. The signal observed at $\delta_6 = 17.1$ ppm at 25 °C and attributed to complex **XIII** is split into two at −16 °C ($\delta = 17.1$ and 17.0 ppm).
[29] a) V. He, V. Gomez, B. Spingler, S. J. Lippard, *Inorg. Chem.* **2000**, *39*, 4188–4189; b) E. W. Ainscough, A. M. Brodie, J. D. Ranford, J. M. Waters, *J. Chem. Soc., Dalton Trans.* **1997**, 1251–1255.

[30] H. I. Park, L.-J. Ming, *Angew. Chem.* **1999**, *111*, 3097–3100; *Angew. Chem. Int. Ed.* **1999**, *38*, 2914–2916.
[31] a) P. Gomez-Tagle, I. Vargas-Zúñiga, O. Taran, A. K. Yatsimirsky, *J. Org. Chem.* **2006**, *71*, 9713–9722; b) P. K. Grzyska, P. G. Czyryca, J. Golightly, K. Small, P. Larsen, R. H. Hoff, A. C. Hengge, *J. Org. Chem.* **2002**, *67*, 1214–1220; c) O. Taran, A. K. Yatsimirsky, *Chem. Commun.* **2004**, 1228–1229.
[32] M. Krack, M. Parrinello, *High Performance Computing in Chemistry, Vol. 25* (Ed.: J. Grotendorst), NIC, Jülich (Germany), **2004**.
[33] S. Torelli, C. Belle, I. Gautier-Luneau, J. L. Pierre, E. Saint-Aman, J. M. Latour, L. Le Pape, D. Luneau, *Inorg. Chem.* **2000**, *39*, 3526–3536.
[34] D. M. Brown, D. A. Usher, *J. Am. Chem. Soc.* **1965**, *87*, 6558–6564; L. Kugel, M. Halmann, *J. Am. Chem. Soc.* **1967**, *89*, 4125–4128.
[35] P. K. Glasoe, F. A. Long, *J. Phys. Chem.* **1960**, *64*, 188–190.
[36] A. D. Becke, *Phys. Rev. A* **1988**, *38*, 3098–3100; C. T. Lee, W. T. Yang, R. G. Parr, *Phys. Rev. B* **1988**, *37*, 785–789.
[37] S. Goedecker, M. Teter, J. Hutter, *Phys. Rev. B* **1996**, *54*, 1703–1710.
[38] A. Altomare, G. Cascarano, C. Giacovazzo, A. Guagliardi, *J. Appl. Crystallogr.* **1993**, *26*, 343–350.
[39] TEXSAN, Single-Crystal Structure Analysis Software, version 1.7, Molecular Structure Corporation, The Woodlands TX, **1995**.
[40] a) A μ-OH complex with the same ligand had previously been structurally characterized, however, a different crystalline form (crystal system and space group) has been obtained in this study, prompting us to detail its molecular structure; b) K. Matsufuji, H. Shiraishi, Y. Miyasato, T. Shiga, M. Ohba, T. Yokoyama, H. Okawa, *Bull. Chem. Soc. Jpn.* **2005**, *78*, 851–858.

Received: January 22, 2007
Published online: August 6, 2007

